

Dalitz plot analysis of the decay $B^\pm \rightarrow K^\pm K^\pm K^\mp$

B. Aubert,¹ R. Barate,¹ M. Bona,¹ D. Boutigny,¹ F. Couderc,¹ Y. Karyotakis,¹ J. P. Lees,¹ V. Poireau,¹
V. Tisserand,¹ A. Zghiche,¹ E. Grauges,² A. Palano,³ M. Pappagallo,³ J. C. Chen,⁴ N. D. Qi,⁴ G. Rong,⁴ P. Wang,⁴
Y. S. Zhu,⁴ G. Eigen,⁵ I. Ofte,⁵ B. Stugu,⁵ G. S. Abrams,⁶ M. Battaglia,⁶ D. N. Brown,⁶ J. Button-Shafer,⁶
R. N. Cahn,⁶ E. Charles,⁶ C. T. Day,⁶ M. S. Gill,⁶ Y. Groysman,⁶ R. G. Jacobsen,⁶ J. A. Kadyk,⁶ L. T. Kerth,⁶
Yu. G. Kolomensky,⁶ G. Kukartsev,⁶ G. Lynch,⁶ L. M. Mir,⁶ P. J. Oddone,⁶ T. J. Orimoto,⁶ M. Pripstein,⁶
N. A. Roe,⁶ M. T. Ronan,⁶ W. A. Wenzel,⁶ M. Barrett,⁷ K. E. Ford,⁷ T. J. Harrison,⁷ A. J. Hart,⁷ C. M. Hawkes,⁷
S. E. Morgan,⁷ A. T. Watson,⁷ K. Goetzen,⁸ T. Held,⁸ H. Koch,⁸ B. Lewandowski,⁸ M. Pelizaeus,⁸ K. Peters,⁸
T. Schroeder,⁸ M. Steinke,⁸ J. T. Boyd,⁹ J. P. Burke,⁹ W. N. Cottingham,⁹ D. Walker,⁹ T. Cuhadar-Donszelmann,¹⁰
B. G. Fulsom,¹⁰ C. Hearty,¹⁰ N. S. Knecht,¹⁰ T. S. Mattison,¹⁰ J. A. McKenna,¹⁰ A. Khan,¹¹ P. Kyberd,¹¹
M. Saleem,¹¹ L. Teodorescu,¹¹ V. E. Blinov,¹² A. D. Bukin,¹² V. P. Druzhinin,¹² V. B. Golubev,¹² A. P. Onuchin,¹²
S. I. Serednyakov,¹² Yu. I. Skovpen,¹² E. P. Solodov,¹² K. Yu Todyshev,¹² D. S. Best,¹³ M. Bondioli,¹³
M. Bruinsma,¹³ M. Chao,¹³ S. Curry,¹³ I. Eschrich,¹³ D. Kirkby,¹³ A. J. Lankford,¹³ P. Lund,¹³ M. Mandelkern,¹³
R. K. Mommsen,¹³ W. Roethel,¹³ D. P. Stoker,¹³ S. Abachi,¹⁴ C. Buchanan,¹⁴ S. D. Foulkes,¹⁵ J. W. Gary,¹⁵
O. Long,¹⁵ B. C. Shen,¹⁵ K. Wang,¹⁵ L. Zhang,¹⁵ H. K. Hadavand,¹⁶ E. J. Hill,¹⁶ H. P. Paar,¹⁶ S. Rahatlou,¹⁶
V. Sharma,¹⁶ J. W. Berryhill,¹⁷ C. Campagnari,¹⁷ A. Cunha,¹⁷ B. Dahmes,¹⁷ T. M. Hong,¹⁷ D. Kovalskiy,¹⁷
J. D. Richman,¹⁷ T. W. Beck,¹⁸ A. M. Eisner,¹⁸ C. J. Flacco,¹⁸ C. A. Heusch,¹⁸ J. Kroseberg,¹⁸ W. S. Lockman,¹⁸
G. Nesom,¹⁸ T. Schalk,¹⁸ B. A. Schumm,¹⁸ A. Seiden,¹⁸ P. Spradlin,¹⁸ D. C. Williams,¹⁸ M. G. Wilson,¹⁸
J. Albert,¹⁹ E. Chen,¹⁹ A. Dvoretzkii,¹⁹ D. G. Hitlin,¹⁹ I. Narsky,¹⁹ T. Piatenko,¹⁹ F. C. Porter,¹⁹ A. Ryd,¹⁹
A. Samuel,¹⁹ R. Andreassen,²⁰ G. Mancinelli,²⁰ B. T. Meadows,²⁰ M. D. Sokoloff,²⁰ F. Blanc,²¹ P. C. Bloom,²¹
S. Chen,²¹ W. T. Ford,²¹ J. F. Hirschauer,²¹ A. Kreisel,²¹ U. Nauenberg,²¹ A. Olivas,²¹ W. O. Ruddick,²¹
J. G. Smith,²¹ K. A. Ulmer,²¹ S. R. Wagner,²¹ J. Zhang,²¹ A. Chen,²² E. A. Eckhart,²² A. Soffer,²² W. H. Toki,²²
R. J. Wilson,²² F. Winklmeier,²² Q. Zeng,²² D. D. Altenburg,²³ E. Feltresi,²³ A. Hauke,²³ H. Jasper,²³ B. Spaan,²³
T. Brandt,²⁴ V. Klose,²⁴ H. M. Lacker,²⁴ W. F. Mader,²⁴ R. Nogowski,²⁴ A. Petzold,²⁴ J. Schubert,²⁴
K. R. Schubert,²⁴ R. Schwierz,²⁴ J. E. Sundermann,²⁴ A. Volk,²⁴ D. Bernard,²⁵ G. R. Bonneaud,²⁵ P. Grenier,^{25,*}
E. Latour,²⁵ Ch. Thiebaux,²⁵ M. Verderi,²⁵ D. J. Bard,²⁶ P. J. Clark,²⁶ W. Gradl,²⁶ F. Muheim,²⁶ S. Playfer,²⁶
A. I. Robertson,²⁶ Y. Xie,²⁶ M. Andreotti,²⁷ D. Bettoni,²⁷ C. Bozzi,²⁷ R. Calabrese,²⁷ G. Cibinetto,²⁷ E. Luppi,²⁷
M. Negrini,²⁷ A. Petrella,²⁷ L. Piemontese,²⁷ E. Prencipe,²⁷ F. Anulli,²⁸ R. Baldini-Feroli,²⁸ A. Calcaterra,²⁸
R. de Sangro,²⁸ G. Finocchiaro,²⁸ S. Pacetti,²⁸ P. Patteri,²⁸ I. M. Peruzzi,^{28,†} M. Piccolo,²⁸ M. Rama,²⁸
A. Zallo,²⁸ A. Buzzo,²⁹ R. Capra,²⁹ R. Contri,²⁹ M. Lo Vetere,²⁹ M. M. Macri,²⁹ M. R. Monge,²⁹ S. Passaggio,²⁹
C. Patrignani,²⁹ E. Robutti,²⁹ A. Santroni,²⁹ S. Tosi,²⁹ G. Brandenburg,³⁰ K. S. Chaisanguanthum,³⁰ M. Morii,³⁰
J. Wu,³⁰ R. S. Dubitzky,³¹ J. Marks,³¹ S. Schenk,³¹ U. Uwer,³¹ W. Bhimji,³² D. A. Bowerman,³² P. D. Dauncey,³²
U. Egede,³² R. L. Flack,³² J. R. Gaillard,³² J. A. Nash,³² M. B. Nikolich,³² W. Panduro Vazquez,³² X. Chai,³³
M. J. Charles,³³ U. Mallik,³³ N. T. Meyer,³³ V. Ziegler,³³ J. Cochran,³⁴ H. B. Crawley,³⁴ L. Dong,³⁴ V. Eyges,³⁴
W. T. Meyer,³⁴ S. Prell,³⁴ E. I. Rosenberg,³⁴ A. E. Rubin,³⁴ A. V. Gritsan,³⁵ M. Fritsch,³⁶ G. Schott,³⁶
N. Arnaud,³⁷ M. Davier,³⁷ G. Grosdidier,³⁷ A. Höcker,³⁷ F. Le Diberder,³⁷ V. Lepeltier,³⁷ A. M. Lutz,³⁷
A. Oyanguren,³⁷ S. Pruvot,³⁷ S. Rodier,³⁷ P. Roudeau,³⁷ M. H. Schune,³⁷ A. Stocchi,³⁷ W. F. Wang,³⁷
G. Wormser,³⁷ C. H. Cheng,³⁸ D. J. Lange,³⁸ D. M. Wright,³⁸ C. A. Chavez,³⁹ I. J. Forster,³⁹ J. R. Fry,³⁹
E. Gabathuler,³⁹ R. Gamet,³⁹ K. A. George,³⁹ D. E. Hutchcroft,³⁹ D. J. Payne,³⁹ K. C. Schofield,³⁹
C. Touramanis,³⁹ A. J. Bevan,⁴⁰ F. Di Lodovico,⁴⁰ W. Menges,⁴⁰ R. Sacco,⁴⁰ C. L. Brown,⁴¹ G. Cowan,⁴¹
H. U. Flaecher,⁴¹ D. A. Hopkins,⁴¹ P. S. Jackson,⁴¹ T. R. McMahon,⁴¹ S. Ricciardi,⁴¹ F. Salvatore,⁴¹ D. N. Brown,⁴²
C. L. Davis,⁴² J. Allison,⁴³ N. R. Barlow,⁴³ R. J. Barlow,⁴³ Y. M. Chia,⁴³ C. L. Edgar,⁴³ M. P. Kelly,⁴³
G. D. Lafferty,⁴³ M. T. Naisbit,⁴³ J. C. Williams,⁴³ J. I. Yi,⁴³ C. Chen,⁴⁴ W. D. Hulsbergen,⁴⁴ A. Jawahery,⁴⁴
C. K. Lae,⁴⁴ D. A. Roberts,⁴⁴ G. Simi,⁴⁴ G. Blaylock,⁴⁵ C. Dallapiccola,⁴⁵ S. S. Hertzbach,⁴⁵ X. Li,⁴⁵ T. B. Moore,⁴⁵
S. Saremi,⁴⁵ H. Staengle,⁴⁵ S. Y. Willocq,⁴⁵ R. Cowan,⁴⁶ K. Koeneke,⁴⁶ G. Sciolla,⁴⁶ S. J. Sekula,⁴⁶ M. Spitznagel,⁴⁶
F. Taylor,⁴⁶ R. K. Yamamoto,⁴⁶ H. Kim,⁴⁷ P. M. Patel,⁴⁷ C. T. Potter,⁴⁷ S. H. Robertson,⁴⁷ A. Lazzaro,⁴⁸
V. Lombardo,⁴⁸ F. Palombo,⁴⁸ J. M. Bauer,⁴⁹ L. Cremaldi,⁴⁹ V. Eschenburg,⁴⁹ R. Godang,⁴⁹ R. Kroeger,⁴⁹
J. Reidy,⁴⁹ D. A. Sanders,⁴⁹ D. J. Summers,⁴⁹ H. W. Zhao,⁴⁹ S. Brunet,⁵⁰ D. Côté,⁵⁰ M. Simard,⁵⁰ P. Taras,⁵⁰
F. B. Viaud,⁵⁰ H. Nicholson,⁵¹ N. Cavallo,^{52,‡} G. De Nardo,⁵² D. del Re,⁵² F. Fabozzi,^{52,‡} C. Gatto,⁵² L. Lista,⁵²

D. Monorchio,⁵² D. Piccolo,⁵² C. Sciacca,⁵² M. Baak,⁵³ H. Bulten,⁵³ G. Raven,⁵³ H. L. Snoek,⁵³ C. P. Jessop,⁵⁴ J. M. LoSecco,⁵⁴ T. Allmendinger,⁵⁵ G. Benelli,⁵⁵ K. K. Gan,⁵⁵ K. Honscheid,⁵⁵ D. Hufnagel,⁵⁵ P. D. Jackson,⁵⁵ H. Kagan,⁵⁵ R. Kass,⁵⁵ T. Pulliam,⁵⁵ A. M. Rahimi,⁵⁵ R. Ter-Antonyan,⁵⁵ Q. K. Wong,⁵⁵ N. L. Blount,⁵⁶ J. Brau,⁵⁶ R. Frey,⁵⁶ O. Igonkina,⁵⁶ M. Lu,⁵⁶ R. Rahmat,⁵⁶ N. B. Sinev,⁵⁶ D. Strom,⁵⁶ J. Strube,⁵⁶ E. Torrence,⁵⁶ F. Galeazzi,⁵⁷ A. Gaz,⁵⁷ M. Margoni,⁵⁷ M. Morandin,⁵⁷ A. Pompili,⁵⁷ M. Posocco,⁵⁷ M. Rotondo,⁵⁷ F. Simonetto,⁵⁷ R. Stroili,⁵⁷ C. Voci,⁵⁷ M. Benayoun,⁵⁸ J. Chauveau,⁵⁸ P. David,⁵⁸ L. Del Buono,⁵⁸ Ch. de la Vaissière,⁵⁸ O. Hamon,⁵⁸ B. L. Hartfiel,⁵⁸ M. J. J. John,⁵⁸ Ph. Leruste,⁵⁸ J. Malcès,⁵⁸ J. Ocariz,⁵⁸ L. Roos,⁵⁸ G. Therin,⁵⁸ P. K. Behera,⁵⁹ L. Gladney,⁵⁹ J. Panetta,⁵⁹ M. Biasini,⁶⁰ R. Covarelli,⁶⁰ M. Pioppi,⁶⁰ C. Angelini,⁶¹ G. Batignani,⁶¹ S. Bettarini,⁶¹ F. Bucci,⁶¹ G. Calderini,⁶¹ M. Carpinelli,⁶¹ R. Cenci,⁶¹ F. Forti,⁶¹ M. A. Giorgi,⁶¹ A. Lusiani,⁶¹ G. Marchiori,⁶¹ M. A. Mazur,⁶¹ M. Morganti,⁶¹ N. Neri,⁶¹ E. Paoloni,⁶¹ G. Rizzo,⁶¹ J. Walsh,⁶¹ M. Haire,⁶² D. Judd,⁶² D. E. Wagoner,⁶² J. Biesiada,⁶³ N. Danielson,⁶³ P. Elmer,⁶³ Y. P. Lau,⁶³ C. Lu,⁶³ J. Olsen,⁶³ A. J. S. Smith,⁶³ A. V. Telnov,⁶³ F. Bellini,⁶⁴ G. Cavoto,⁶⁴ A. D’Orazio,⁶⁴ E. Di Marco,⁶⁴ R. Faccini,⁶⁴ F. Ferrarotto,⁶⁴ F. Ferroni,⁶⁴ M. Gaspero,⁶⁴ L. Li Gioi,⁶⁴ M. A. Mazzoni,⁶⁴ S. Morganti,⁶⁴ G. Piredda,⁶⁴ F. Polci,⁶⁴ F. Safai Tehrani,⁶⁴ C. Voena,⁶⁴ M. Ebert,⁶⁵ H. Schröder,⁶⁵ R. Waldi,⁶⁵ T. Adye,⁶⁶ N. De Groot,⁶⁶ B. Franek,⁶⁶ E. O. Olaiya,⁶⁶ F. F. Wilson,⁶⁶ S. Emery,⁶⁷ A. Gaidot,⁶⁷ S. F. Ganzhur,⁶⁷ G. Hamel de Monchenault,⁶⁷ W. Kozanecki,⁶⁷ M. Legendre,⁶⁷ B. Mayer,⁶⁷ G. Vasseur,⁶⁷ Ch. Yèche,⁶⁷ M. Zito,⁶⁷ W. Park,⁶⁸ M. V. Purohit,⁶⁸ A. W. Weidemann,⁶⁸ J. R. Wilson,⁶⁸ M. T. Allen,⁶⁹ D. Aston,⁶⁹ R. Bartoldus,⁶⁹ P. Bechtel,⁶⁹ N. Berger,⁶⁹ A. M. Boyarski,⁶⁹ R. Claus,⁶⁹ J. P. Coleman,⁶⁹ M. R. Convery,⁶⁹ M. Cristinziani,⁶⁹ J. C. Dingfelder,⁶⁹ D. Dong,⁶⁹ J. Dorfan,⁶⁹ G. P. Dubois-Felsmann,⁶⁹ D. Dujmic,⁶⁹ W. Dunwoodie,⁶⁹ R. C. Field,⁶⁹ T. Glanzman,⁶⁹ S. J. Gowdy,⁶⁹ M. T. Graham,⁶⁹ V. Halyo,⁶⁹ C. Hast,⁶⁹ T. Hryn’ova,⁶⁹ W. R. Innes,⁶⁹ M. H. Kelsey,⁶⁹ P. Kim,⁶⁹ M. L. Kocian,⁶⁹ D. W. G. S. Leith,⁶⁹ S. Li,⁶⁹ J. Libby,⁶⁹ S. Luitz,⁶⁹ V. Luth,⁶⁹ H. L. Lynch,⁶⁹ D. B. MacFarlane,⁶⁹ H. Marsiske,⁶⁹ R. Messner,⁶⁹ D. R. Muller,⁶⁹ C. P. O’Grady,⁶⁹ V. E. Ozcan,⁶⁹ A. Perazzo,⁶⁹ M. Perl,⁶⁹ B. N. Ratcliff,⁶⁹ A. Roodman,⁶⁹ A. A. Salnikov,⁶⁹ R. H. Schindler,⁶⁹ J. Schwiening,⁶⁹ A. Snyder,⁶⁹ J. Stelzer,⁶⁹ D. Su,⁶⁹ M. K. Sullivan,⁶⁹ K. Suzuki,⁶⁹ S. K. Swain,⁶⁹ J. M. Thompson,⁶⁹ J. Va’vra,⁶⁹ N. van Bakel,⁶⁹ M. Weaver,⁶⁹ A. J. R. Weinstein,⁶⁹ W. J. Wisniewski,⁶⁹ M. Wittgen,⁶⁹ D. H. Wright,⁶⁹ A. K. Yarritu,⁶⁹ K. Yi,⁶⁹ C. C. Young,⁶⁹ P. R. Burchat,⁷⁰ A. J. Edwards,⁷⁰ S. A. Majewski,⁷⁰ B. A. Petersen,⁷⁰ C. Roat,⁷⁰ L. Wilden,⁷⁰ S. Ahmed,⁷¹ M. S. Alam,⁷¹ R. Bula,⁷¹ J. A. Ernst,⁷¹ V. Jain,⁷¹ B. Pan,⁷¹ M. A. Saeed,⁷¹ F. R. Wappler,⁷¹ S. B. Zain,⁷¹ W. Bugg,⁷² M. Krishnamurthy,⁷² S. M. Spanier,⁷² R. Eckmann,⁷³ J. L. Ritchie,⁷³ A. Satpathy,⁷³ C. J. Schilling,⁷³ R. F. Schwitters,⁷³ J. M. Izen,⁷⁴ I. Kitayama,⁷⁴ X. C. Lou,⁷⁴ S. Ye,⁷⁴ F. Bianchi,⁷⁵ F. Gallo,⁷⁵ D. Gamba,⁷⁵ M. Bomben,⁷⁶ L. Bosisio,⁷⁶ C. Cartaro,⁷⁶ F. Cossutti,⁷⁶ G. Della Ricca,⁷⁶ S. Dittongo,⁷⁶ S. Grancagnolo,⁷⁶ L. Lancieri,⁷⁶ L. Vitale,⁷⁶ V. Azzolini,⁷⁷ F. Martinez-Vidal,⁷⁷ Sw. Banerjee,⁷⁸ B. Bhuyan,⁷⁸ C. M. Brown,⁷⁸ D. Fortin,⁷⁸ K. Hamano,⁷⁸ R. Kowalewski,⁷⁸ I. M. Nugent,⁷⁸ J. M. Roney,⁷⁸ R. J. Sobie,⁷⁸ J. J. Back,⁷⁹ P. F. Harrison,⁷⁹ T. E. Latham,⁷⁹ G. B. Mohanty,⁷⁹ H. R. Band,⁸⁰ X. Chen,⁸⁰ B. Cheng,⁸⁰ S. Dasu,⁸⁰ M. Datta,⁸⁰ A. M. Eichenbaum,⁸⁰ K. T. Flood,⁸⁰ J. J. Hollar,⁸⁰ J. R. Johnson,⁸⁰ P. E. Kutter,⁸⁰ H. Li,⁸⁰ R. Liu,⁸⁰ B. Mellado,⁸⁰ A. Mihalyi,⁸⁰ A. K. Mohapatra,⁸⁰ Y. Pan,⁸⁰ M. Pierini,⁸⁰ R. Prepost,⁸⁰ P. Tan,⁸⁰ S. L. Wu,⁸⁰ Z. Yu,⁸⁰ and H. Neal⁸¹

(The BABAR Collaboration)

¹Laboratoire de Physique des Particules, F-74941 Annecy-le-Vieux, France

²Universitat de Barcelona Fac. Fisica. Dept. ECM Avda Diagonal 647, 6a planta E-08028 Barcelona, Spain

³Università di Bari, Dipartimento di Fisica and INFN, I-70126 Bari, Italy

⁴Institute of High Energy Physics, Beijing 100039, China

⁵University of Bergen, Institute of Physics, N-5007 Bergen, Norway

⁶Lawrence Berkeley National Laboratory and University of California, Berkeley, California 94720, USA

⁷University of Birmingham, Birmingham, B15 2TT, United Kingdom

⁸Ruhr Universität Bochum, Institut für Experimentalphysik 1, D-44780 Bochum, Germany

⁹University of Bristol, Bristol BS8 1TL, United Kingdom

¹⁰University of British Columbia, Vancouver, British Columbia, Canada V6T 1Z1

¹¹Brunel University, Uxbridge, Middlesex UB8 3PH, United Kingdom

¹²Budker Institute of Nuclear Physics, Novosibirsk 630090, Russia

¹³University of California at Irvine, Irvine, California 92697, USA

¹⁴University of California at Los Angeles, Los Angeles, California 90024, USA

¹⁵University of California at Riverside, Riverside, California 92521, USA

¹⁶University of California at San Diego, La Jolla, California 92093, USA

¹⁷University of California at Santa Barbara, Santa Barbara, California 93106, USA

¹⁸University of California at Santa Cruz, Institute for Particle Physics, Santa Cruz, California 95064, USA

¹⁹California Institute of Technology, Pasadena, California 91125, USA

²⁰University of Cincinnati, Cincinnati, Ohio 45221, USA

- ²¹ University of Colorado, Boulder, Colorado 80309, USA
- ²² Colorado State University, Fort Collins, Colorado 80523, USA
- ²³ Universität Dortmund, Institut für Physik, D-44221 Dortmund, Germany
- ²⁴ Technische Universität Dresden, Institut für Kern- und Teilchenphysik, D-01062 Dresden, Germany
- ²⁵ Ecole Polytechnique, LLR, F-91128 Palaiseau, France
- ²⁶ University of Edinburgh, Edinburgh EH9 3JZ, United Kingdom
- ²⁷ Università di Ferrara, Dipartimento di Fisica and INFN, I-44100 Ferrara, Italy
- ²⁸ Laboratori Nazionali di Frascati dell'INFN, I-00044 Frascati, Italy
- ²⁹ Università di Genova, Dipartimento di Fisica and INFN, I-16146 Genova, Italy
- ³⁰ Harvard University, Cambridge, Massachusetts 02138, USA
- ³¹ Universität Heidelberg, Physikalisches Institut, Philosophenweg 12, D-69120 Heidelberg, Germany
- ³² Imperial College London, London, SW7 2AZ, United Kingdom
- ³³ University of Iowa, Iowa City, Iowa 52242, USA
- ³⁴ Iowa State University, Ames, Iowa 50011-3160, USA
- ³⁵ Johns Hopkins Univ. Dept of Physics & Astronomy 3400 N. Charles Street Baltimore, Maryland 21218
- ³⁶ Universität Karlsruhe, Institut für Experimentelle Kernphysik, D-76021 Karlsruhe, Germany
- ³⁷ Laboratoire de l'Accélérateur Linéaire, IN2P3-CNRS et Université Paris-Sud 11, Centre Scientifique d'Orsay, B.P. 34, F-91898 ORSAY Cedex, France
- ³⁸ Lawrence Livermore National Laboratory, Livermore, California 94550, USA
- ³⁹ University of Liverpool, Liverpool L69 7ZE, United Kingdom
- ⁴⁰ Queen Mary, University of London, E1 4NS, United Kingdom
- ⁴¹ University of London, Royal Holloway and Bedford New College, Egham, Surrey TW20 0EX, United Kingdom
- ⁴² University of Louisville, Louisville, Kentucky 40292, USA
- ⁴³ University of Manchester, Manchester M13 9PL, United Kingdom
- ⁴⁴ University of Maryland, College Park, Maryland 20742, USA
- ⁴⁵ University of Massachusetts, Amherst, Massachusetts 01003, USA
- ⁴⁶ Massachusetts Institute of Technology, Laboratory for Nuclear Science, Cambridge, Massachusetts 02139, USA
- ⁴⁷ McGill University, Montréal, Québec, Canada H3A 2T8
- ⁴⁸ Università di Milano, Dipartimento di Fisica and INFN, I-20133 Milano, Italy
- ⁴⁹ University of Mississippi, University, Mississippi 38677, USA
- ⁵⁰ Université de Montréal, Physique des Particules, Montréal, Québec, Canada H3C 3J7
- ⁵¹ Mount Holyoke College, South Hadley, Massachusetts 01075, USA
- ⁵² Università di Napoli Federico II, Dipartimento di Scienze Fisiche and INFN, I-80126, Napoli, Italy
- ⁵³ NIKHEF, National Institute for Nuclear Physics and High Energy Physics, NL-1009 DB Amsterdam, The Netherlands
- ⁵⁴ University of Notre Dame, Notre Dame, Indiana 46556, USA
- ⁵⁵ Ohio State University, Columbus, Ohio 43210, USA
- ⁵⁶ University of Oregon, Eugene, Oregon 97403, USA
- ⁵⁷ Università di Padova, Dipartimento di Fisica and INFN, I-35131 Padova, Italy
- ⁵⁸ Universités Paris VI et VII, Laboratoire de Physique Nucléaire et de Hautes Energies, F-75252 Paris, France
- ⁵⁹ University of Pennsylvania, Philadelphia, Pennsylvania 19104, USA
- ⁶⁰ Università di Perugia, Dipartimento di Fisica and INFN, I-06100 Perugia, Italy
- ⁶¹ Università di Pisa, Dipartimento di Fisica, Scuola Normale Superiore and INFN, I-56127 Pisa, Italy
- ⁶² Prairie View A&M University, Prairie View, Texas 77446, USA
- ⁶³ Princeton University, Princeton, New Jersey 08544, USA
- ⁶⁴ Università di Roma La Sapienza, Dipartimento di Fisica and INFN, I-00185 Roma, Italy
- ⁶⁵ Universität Rostock, D-18051 Rostock, Germany
- ⁶⁶ Rutherford Appleton Laboratory, Chilton, Didcot, Oxon, OX11 0QX, United Kingdom
- ⁶⁷ DSM/Dapnia, CEA/Saclay, F-91191 Gif-sur-Yvette, France
- ⁶⁸ University of South Carolina, Columbia, South Carolina 29208, USA
- ⁶⁹ Stanford Linear Accelerator Center, Stanford, California 94309, USA
- ⁷⁰ Stanford University, Stanford, California 94305-4060, USA
- ⁷¹ State University of New York, Albany, New York 12222, USA
- ⁷² University of Tennessee, Knoxville, Tennessee 37996, USA
- ⁷³ University of Texas at Austin, Austin, Texas 78712, USA
- ⁷⁴ University of Texas at Dallas, Richardson, Texas 75083, USA
- ⁷⁵ Università di Torino, Dipartimento di Fisica Sperimentale and INFN, I-10125 Torino, Italy
- ⁷⁶ Università di Trieste, Dipartimento di Fisica and INFN, I-34127 Trieste, Italy
- ⁷⁷ IFIC, Universitat de Valencia-CSIC, E-46071 Valencia, Spain
- ⁷⁸ University of Victoria, Victoria, British Columbia, Canada V8W 3P6
- ⁷⁹ Department of Physics, University of Warwick, Coventry CV4 7AL, United Kingdom
- ⁸⁰ University of Wisconsin, Madison, Wisconsin 53706, USA
- ⁸¹ Yale University, New Haven, Connecticut 06511, USA

(Dated: October 1, 2018)

We analyze the three-body charmless decay $B^\pm \rightarrow K^\pm K^\pm K^\mp$ using a sample of 226.0 ± 2.5 million $B\bar{B}$ pairs collected by the *BABAR* detector. We measure the total branching fraction and CP asymmetry to be $\mathcal{B} = (35.2 \pm 0.9 \pm 1.6) \times 10^{-6}$ and $A_{CP} = (-1.7 \pm 2.6 \pm 1.5)\%$. We fit the Dalitz plot distribution using an isobar model and measure the magnitudes and phases of the decay coefficients. We find no evidence of CP violation for the individual components of the isobar model. The decay dynamics is dominated by the K^+K^- S -wave, for which we perform a partial-wave analysis in the region $m(K^+K^-) < 2 \text{ GeV}/c^2$. Significant production of the $f_0(980)$ resonance, and of a spin zero state near $1.55 \text{ GeV}/c^2$ are required in the isobar model description of the data. The partial-wave analysis supports this observation.

PACS numbers: 13.25.Hw, 11.30.Er, 11.80.Et

I. INTRODUCTION

Charmless decays of B mesons provide a rich laboratory for studying different aspects of weak and strong interactions. With recent theoretical progress in understanding the strong interaction effects, specific predictions for two-body pseudoscalar-pseudoscalar, $B \rightarrow PP$, and pseudoscalar-vector, $B \rightarrow PV$, branching fractions and asymmetries are available [1, 2, 3, 4] and global fits to experimental data have been performed [5, 6]. Improved experimental measurements of a comprehensive set of charmless B decays coupled with further theoretical progress hold the potential to provide significant constraints on the CKM matrix parameters and to discover hints of physics beyond the Standard Model in penguin-mediated $b \rightarrow s$ transitions.

We analyze the decay $B^\pm \rightarrow K^\pm K^\pm K^\mp$, dominated by the $b \rightarrow s$ penguin-loop transition, using 226.0 ± 2.5 million $B\bar{B}$ pairs collected by the *BABAR* detector [7] at the SLAC PEP-II asymmetric-energy B factory [8] operating at the $\Upsilon(4S)$ resonance. *BABAR* has previously measured the total branching fraction and asymmetry in this mode [9] and the two-body branching fractions $B^\pm \rightarrow K^\pm \phi(1020)$, $B^\pm \rightarrow K^\pm \chi_{c0}$ [10, 11]. A comprehensive Dalitz plot analysis of $B^\pm \rightarrow K^\pm K^\pm K^\mp$ has been published by the Belle collaboration [12].

II. EVENT SELECTION

We consider events with at least four reliably reconstructed charged-particle tracks consistent with having originated from the interaction point. All three tracks forming a $B^\pm \rightarrow K^\pm K^\pm K^\mp$ decay candidate are required to be consistent with a kaon hypothesis using a particle identification algorithm that has an average efficiency of 94% within the acceptance of the detector and an average pion-to-kaon misidentification probability of 6%.

We use two kinematic variables to identify the signal. The first is $\Delta E = E - \sqrt{s_0}/2$, the difference between the reconstructed B candidate energy and half the energy of the e^+e^- initial state, both in the e^+e^- center-of-mass (CM) frame. For signal events the ΔE distribution peaks near zero with a resolution of 21 MeV. We require the candidates to have $|\Delta E| < 40 \text{ MeV}$. The second variable is the energy-substituted mass $m_{\text{ES}} = \sqrt{(s_0/2 + \mathbf{p}_0 \cdot \mathbf{p}_B)^2/E_0^2 - \mathbf{p}_B^2}$, where \mathbf{p}_B is the momentum of the B candidate and (E_0, \mathbf{p}_0) is the four-momentum of the e^+e^- initial state, both in the laboratory frame. For signal events the m_{ES} distribution peaks near the B mass with a resolution of $2.6 \text{ MeV}/c^2$. We define a signal region (SR) with $m_{\text{ES}} \in (5.27, 5.29) \text{ GeV}/c^2$ and a sideband (SB) with $m_{\text{ES}} \in (5.20, 5.25) \text{ GeV}/c^2$.

The dominant background is due to events from light-quark or charm continuum production, $e^+e^- \rightarrow q\bar{q}$, whose jet-like event topology is different from the more spherical B decays. We suppress this continuum background by requiring the absolute value of the cosine of the angle between the thrust axes of the B candidate and the rest of the event in the CM frame to be smaller than 0.95. Further suppression is achieved using a neural network with four inputs computed in the CM frame: the cosine of the angle between the direction of the B candidate and the beam direction; the absolute value of the cosine of the angle between the candidate thrust axis and the beam direction; and momentum-weighted sums over tracks and neutral clusters not belonging to the candidate, $\sum_i p_i$ and $\sum_i p_i \cos^2 \theta_i$, where p_i is the track momentum and θ_i is the angle between the track momentum direction and the candidate thrust axis.

Figure 1 shows the m_{ES} distribution of the 9870 events thus selected. The histogram is fitted with a sum of a Gaussian distribution and a background function having a probability density, $P(x) \propto x\sqrt{1-x^2} \exp(-\xi(1-x^2))$, where $x = 2m_{\text{ES}}/\sqrt{s_0}$ and ξ is a shape parameter [13]. The binned maximum likelihood fit gives $\chi^2 = 104$ for 100 bins and $\xi = 21.1 \pm 1.6$. The ratio of the integrals of the background function over the signal region and the sideband yields an extrapolation coefficient $R_{q\bar{q}} = 0.231 \pm 0.007$. The expected number of $q\bar{q}$ background events in the signal region is $n_{q\bar{q}}^{\text{SR}} = R_{q\bar{q}}(n^{\text{SB}} - n_{B\bar{B}}^{\text{SB}}) = 972 \pm 34$, where $n^{\text{SB}} = 4659$ is the number of events in the sideband from which we subtract the number of non-signal $B\bar{B}$ background events $n_{B\bar{B}}^{\text{SB}} = 431 \pm 19$, estimated

*Also at Laboratoire de Physique Corpusculaire, Clermont-Ferrand, France

†Also with Università di Perugia, Dipartimento di Fisica, Perugia, Italy

‡Also with Università della Basilicata, Potenza, Italy

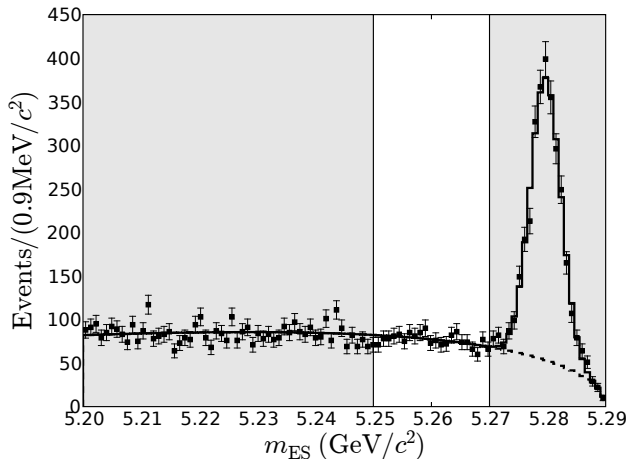


FIG. 1: The m_{ES} distribution of the 9870 selected events, shown as the data points with statistical errors. The solid histogram shows a fit with a sum of a Gaussian distribution ($m_0 = 5.2797 \pm 0.0007 \text{ GeV}/c^2$, $\sigma = 2.64 \pm 0.07 \text{ MeV}/c^2$, $N = 2394 \pm 63$) and a background function [13], shown as a dashed histogram. The shaded regions correspond to the signal region and the m_{ES} sideband defined in the text.

using a large number of simulated exclusive B decays. The expected number of $B\bar{B}$ background events in the signal region is $n_{B\bar{B}}^{SR} = 276 \pm 20$, with $B^\pm \rightarrow DK^\pm$ decays giving the largest contribution.

We use a kinematic fit, constraining the mass of the selected candidates to the mass of the B meson. The three-body decay kinematics is described by two independent di-kaon invariant mass variables $(m_{23}^2, m_{13}^2) = (s_{23}, s_{13})$, where we order the same-sign kaons such that $s_{23} \leq s_{13}$. The signal region contains 1769 B^+ and 1730 B^- candidates whose Dalitz plot distribution is shown in Fig. 2.

III. ISOBAR MODEL FIT

We perform an extended binned maximum likelihood fit to the event distribution in Fig. 2 by binning the folded Dalitz plot into 292 non-uniform rectangular bins and minimizing the log of the Poisson likelihood ratio, $\chi_{LLR}^2/2 = \sum_{i=1}^{292} \mu_i - n_i^{SR} + n_i^{SR} \ln(n_i^{SR}/\mu_i)$, where n_i^{SR} is the number of observed signal region events in the i -th bin, assumed to be sampled from a Poisson distribution with mean μ_i . In the limit of large statistics, the χ_{LLR}^2 function has a χ^2 distribution and can be used to evaluate the goodness-of-fit.

The expected number of events in the i -th bin is modeled as

$$\mu_i = 2 \int_i \epsilon |\mathcal{M}|^2 dm_{23}^2 dm_{13}^2 + R_{q\bar{q}}(n_i^{SB} - n_{iB\bar{B}}^{SB}) + n_{iB\bar{B}}^{SR}, \quad (1)$$

where the first term is the expected signal contribution, given by twice the bin integral of the square of the matrix

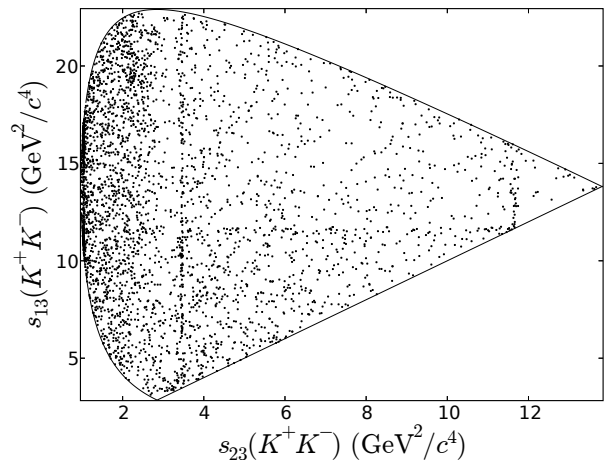


FIG. 2: The Dalitz plot of the 1769 B^+ and 1730 B^- candidates selected in the signal m_{ES} region. The axes are defined in the text.

element multiplied by the signal selection efficiency ϵ , determined as a function of (m_{23}, m_{13}) using simulated signal events. The integral is multiplied by two because we use a folded Dalitz plot. We use the isobar model formalism [14, 15] and describe the matrix element \mathcal{M} as a sum of coherent contributions, $\mathcal{M} = \sum_{k=1}^N \mathcal{M}_k$. The individual contributions are symmetrized with respect to the interchange of same-sign kaons, $1 \leftrightarrow 2$, and are given by

$$\mathcal{M}_k = \frac{\rho_k e^{i\phi_k}}{\sqrt{2}} (\mathcal{A}_k(s_{23}) P_{J_k}(\cos \theta_{13}) + \{1 \leftrightarrow 2\}), \quad (2)$$

where $\rho_k e^{i\phi_k}$ is a complex-valued decay coefficient, \mathcal{A}_k is the amplitude describing a K^+K^- system in a state with angular momentum J and invariant mass $\sqrt{s_{23}}$, P_J is the Legendre polynomial of order J , and the helicity angle θ_{13} between the direction of the bachelor recoil kaon 1 and kaon 3 is measured in the rest frame of kaons 2 and 3.

The model includes contributions from the $\phi(1020)$ and χ_{c0} intermediate resonances, which are clearly visible in Fig. 2. Following Ref. [12], we introduce a broad scalar resonance, whose interference with a slowly varying non-resonant component is used to describe the rapid decrease in event density around $m(K^+K^-) = 1.6 \text{ GeV}/c^2$. Evidence of a possible resonant S -wave contribution in this region has been reported previously [16, 17], however its attribution is uncertain: the $f_0(1370)$ and $f_0(1500)$ resonances are known to couple more strongly to $\pi\pi$ than to $K\bar{K}$ [18]; possible interpretations in terms of those states [19] must account for the fact that no strong $B^\pm \rightarrow K^\pm f_0(1370)$ or $B^\pm \rightarrow K^\pm f_0(1500)$ signal is observed in $B^\pm \rightarrow K^\pm \pi^\pm \pi^\mp$ [12, 20]. The contribution of the $f_0(1710)$ resonance is included in the fit as a separate component and is found to be small. In the following, we

designate the broad scalar resonance $X_0(1550)$ and determine its mass and width directly from the fit.

The contribution from a spin J resonance with mass m_0 and total width Γ_0 is described by a relativistic Breit-Wigner amplitude:

$$\mathcal{A}_J(s) = \frac{F_J(q_{K^\pm}R)}{m_0^2 - s - im_0(\Gamma_0 + \Delta\Gamma(s))}. \quad (3)$$

F_J is the Blatt-Weisskopf centrifugal barrier factor [21] for angular momentum J : $F_0(x) \equiv 1$ and $F_1(x) \equiv x/\sqrt{1+x^2}$, $q_h = \sqrt{s/4 - m_h^2}$, and R represents the effective radius of the interaction volume for the resonance; we use $R = 4.0 \text{ GeV}^{-1}$ (0.8 fm) [22]. In the formulation of Eq. (3), only the centrifugal barrier factor for the decay of a spin J resonance into two pseudoscalar kaons is included; we have ignored the corresponding centrifugal barrier factor for the two-body decay of a B meson into a pseudoscalar kaon and a spin J resonance. The effect of this approximation on the parameterization of $B^\pm \rightarrow K^\pm \phi(1020)$, the only component with $J > 0$, is negligible. Unless otherwise specified, all resonance parameters are taken from Ref. [18]. The term $\Delta\Gamma(s)$, parameterizing the mass dependence of the total width, is in general given by $\Delta\Gamma(s) = \sum_i \Delta\Gamma_i(s)$, where the sum is over all decay modes of the resonance, and $\Delta\Gamma_i(m_0^2) \equiv 0$. The χ_{c0} has many decay modes, the decay modes of the $f_0(1710)$ are not well established, and decay modes other than K^+K^- of the possible $X_0(1550)$ resonance are unknown; in all these cases we set $\Delta\Gamma(s) = 0$ and neglect the mass dependence of the total width. For the $\phi(1020)$ resonance we use $\Delta\Gamma(s) = \Delta\Gamma_1(s) + \Delta\Gamma_2(s)$, where $\Gamma_1 = \Gamma_0 \mathcal{B}(\phi \rightarrow K^+K^-)$, $\Gamma_2 = \Gamma_0 \mathcal{B}(\phi \rightarrow K^0\bar{K}^0)$, and the mass dependence of the partial width for the two-body vector to pseudoscalar-pseudoscalar decay $\phi(1020) \rightarrow h\bar{h}$ is parameterized as

$$\Delta\Gamma_{1,2}(s) = \Gamma_{1,2} \left(\frac{q_h}{q_{0h}} \frac{m_\phi}{\sqrt{s}} \frac{F_1^2(q_h R)}{F_1^2(q_{0h} R)} - 1 \right), \quad (4)$$

where $q_{0h} = \sqrt{m_\phi^2/4 - m_h^2}$.

A large $B^\pm \rightarrow K^\pm f_0(980)$ signal measured in $B^\pm \rightarrow K^\pm \pi^\pm \pi^\mp$ [12, 20], and a recent measurement of g_K/g_π , the ratio of the $f_0(980)$ coupling constants to $K\bar{K}$ and $\pi\pi$ [23], motivate us to include an $f_0(980)$ contribution using a coupled-channel amplitude parameterization:

$$\mathcal{A}_{f_0(980)}(s) = \frac{1}{m_0^2 - s - im_0(g_\pi \varrho_\pi + g_K \varrho_K)}, \quad (5)$$

where $\varrho_\pi = 2/3\sqrt{1 - 4m_\pi^2/s} + 1/3\sqrt{1 - 4m_{\pi^0}^2/s}$, $\varrho_K = 1/2\sqrt{1 - 4m_{K^\pm}^2/s} + 1/2\sqrt{1 - 4m_{K^0}^2/s}$, and we use $g_K/g_\pi = 4.21 \pm 0.25 \pm 0.21$, $m_0 = 0.965 \pm 0.008 \pm 0.006 \text{ GeV}/c^2$ and $g_\pi = 0.165 \pm 0.010 \pm 0.015 \text{ GeV}/c^2$ [23].

We have investigated two theoretical models of the nonresonant component [24, 25] and found that neither

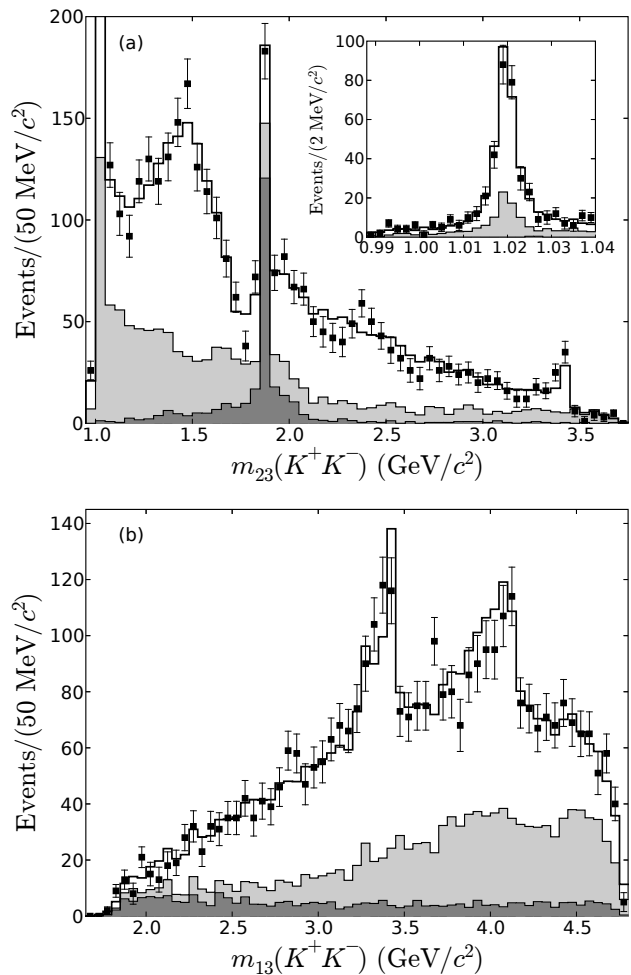


FIG. 3: The projected $m(K^+K^-)$ invariant-mass distributions for the best fit: (a) m_{23} projection (the inset shows the fit projection near the $\phi(1020)$ resonance), (b) m_{13} projection. The histograms show the result of the fit with $B\bar{B}$ and $q\bar{q}$ background contributions shown in dark and light gray, respectively.

describes the data adequately. We therefore include an S -wave nonresonant component expanded beyond the usual constant term as

$$\mathcal{M}_{\text{NR}} = \frac{\rho_{\text{NR}} e^{i\phi_{\text{NR}}}}{\sqrt{2}} \left(e^{-(\alpha+i\beta)s_{23}} + e^{-(\alpha+i\beta)s_{13}} \right). \quad (6)$$

A fit to the $m_{23} > 2 \text{ GeV}/c^2$ region of the folded Dalitz plot of Fig 2, which is dominated by the nonresonant component, gives $\alpha = 0.140 \pm 0.019 \text{ GeV}^{-2}c^4$, $\beta = -0.02 \pm 0.06 \text{ GeV}^{-2}c^4$, consistent with no phase variation. In the following we fix $\beta = 0$, and incorporate the \mathcal{M}_{NR} contribution over the entire Dalitz plot, thus effectively employing the same parameterization as in Ref. [12].

We fit for the magnitudes and phases of the decay coefficients, the mass and width of the $X_0(1550)$, and the nonresonant component shape parameter α . As the overall complex phase of the isobar model amplitude is arbi-

trary, we fix the phase of the nonresonant contribution to zero, leaving 14 free parameters in the fit. The number of degrees of freedom is $292 - 14 = 278$. We perform multiple minimizations with different starting points and find multiple solutions clustered in pairs, where the solutions within each pair are very similar, except for the magnitude and phase of the χ_{c0} decay coefficient. The twofold ambiguity arises from the interference between the narrow χ_{c0} and the nonresonant component, which is approximately constant across the resonance. The highest-likelihood pair has $\chi_{\text{LLR}}^2 = (346.4, 352.0)$; the second best pair has $\chi_{\text{LLR}}^2 = (362.4, 368.7)$. The least significant components are the $f_0(980)$ and the $f_0(1710)$. Their omission from the fit model degrades the best fit from $\chi_{\text{LLR}}^2 = 346.4$ to 363.9 and 360.7, respectively.

The invariant-mass projections of the best fit are shown in Fig. 3. The goodness-of-fit is $\chi^2 = 56$ for 56 bins in the m_{23} projection and $\chi^2 = 66$ for 63 bins in the m_{13} projection. The sharp peak in the $B\bar{B}$ background distribution in the m_{23} projection is due to the contribution from the $B^\pm \rightarrow DK^\pm$ backgrounds. The fit gives $\alpha = 0.152 \pm 0.011 \text{ GeV}^{-2} c^4$, $m_0(X_0) = 1.539 \pm 0.020 \text{ GeV}/c^2$, and $\Gamma_0(X_0) = 0.257 \pm 0.033 \text{ GeV}/c^2$. The fitted values of the shape parameter α and the resonance mass are consistent with the values in Ref. [12], but our preferred value for the width is significantly larger. The results of the best isobar model fit are summarized in Table I, where we have also included the results for the χ_{c0} component from the second solution in the highest-likelihood pair, labeled χ_{c0}^{II} , and component fit fractions,

$$F_k = \frac{\int |\mathcal{M}_k|^2 ds_{23} ds_{13}}{\int |\mathcal{M}|^2 ds_{23} ds_{13}}, \quad (7)$$

where the integrals are taken over the entire Dalitz plot. The sum of the component fit fractions is significantly larger than one due to large negative interference in the scalar sector [26].

IV. BRANCHING FRACTIONS AND ASYMMETRIES

To search for possible direct CP violation we extend the isobar model formalism by defining charge-dependent decay coefficients:

$$\rho_k^\mp e^{i\phi_k^\mp} = \rho_k e^{i\phi_k} \sqrt{\frac{1 \pm A_k}{2}} e^{\pm i\delta\phi_k/2}, \quad (8)$$

where A_k is the CP asymmetry of the k -th component, and $\delta\phi_k = \phi_k^- - \phi_k^+$. We modify the likelihood to be the product of the likelihoods for the two charges and repeat the fit. The phase of the nonresonant component is fixed to zero for both charges. The results are given in the last three columns of Table I in terms of the fitted CP asymmetry values, the symmetric 90% confidence level intervals around them, and the fitted phase differences between the charge-dependent decay coefficients.

The asymmetry intervals are estimated by fitting Monte Carlo simulated samples generated according to the parameterized model of the nominal asymmetry fit. There is no evidence of statistically significant CP violation for any of the components.

Taking into account the signal Dalitz plot distribution, as described by the isobar model fit, the average signal efficiency is $\bar{\varepsilon} = 0.282 \pm 0.011$, where the uncertainty is evaluated using control data samples, and is primarily due to the uncertainties in tracking and particle identification efficiencies. The total branching fraction is $\mathcal{B}(B^\pm \rightarrow K^\pm K^\pm K^\mp) = (35.2 \pm 0.9 \pm 1.6) \times 10^{-6}$, where the first error is statistical and the second is systematic. The fit fraction of the isobar model terms that do not involve the χ_{c0} resonance is $(95.0 \pm 0.6 \pm 1.1)\%$ for the best fit, giving $\mathcal{B}(B^\pm \rightarrow K^\pm K^\pm K^\mp) = (33.5 \pm 0.9 \pm 1.6) \times 10^{-6}$ if intrinsic charm contributions are excluded. The total asymmetry is $A_{CP} = \frac{\mathcal{B}(B^- \rightarrow K^- K^- K^+) - \mathcal{B}(B^+ \rightarrow K^+ K^+ K^-)}{\mathcal{B}(B^- \rightarrow K^- K^- K^+) + \mathcal{B}(B^+ \rightarrow K^+ K^+ K^-)} = (-1.7 \pm 2.6 \pm 1.5)\%$.

The systematic error for the overall branching fraction is obtained by combining in quadrature the 3.9% efficiency uncertainty, a 1.1% uncertainty on the total number of $B^+ B^-$ pairs, a 0.7% uncertainty due to the modeling of $B\bar{B}$ backgrounds, and a 1.4% uncertainty due to the uncertainty arising from the uncertainty on the $R_{q\bar{q}}$ sideband extrapolation coefficient. The 1.5% systematic uncertainty for the asymmetry is due to possible charge asymmetry in kaon tracking and particle identification efficiencies, evaluated using data control samples. Where appropriate, the systematic uncertainties discussed above have been propagated to estimate the uncertainties on the leading isobar model fit results. We have also evaluated the systematic uncertainties due to the parameterization of resonance lineshapes by varying the parameters of all resonances within their respective uncertainties. Uncertainties arising from the distortion of narrow resonance lineshapes due to finite detector resolution and, for candidates containing a $\phi(1020)$ resonance produced in the $q\bar{q}$ continuum, due to the kinematic fit, have also been studied.

The values of the partial two-body branching fractions are summarized in the fifth column of Table I. Using the $\mathcal{B}(\phi(1020) \rightarrow K^+ K^-)$ and $\mathcal{B}(\chi_{c0} \rightarrow K^+ K^-)$ branching fractions from Ref. [18], we compute $\mathcal{B}(B^\pm \rightarrow K^\pm \phi(1020)) = (8.4 \pm 0.7 \pm 0.7 \pm 0.1) \times 10^{-6}$ and $\mathcal{B}(B^\pm \rightarrow K^\pm \chi_{c0}) = (1.84 \pm 0.32 \pm 0.14 \pm 0.28) \times 10^{-4}$, where the last error is due to the uncertainty on the $\phi(1020)$ and χ_{c0} branching fractions. Both results are in agreement with previous measurements [10, 11, 12, 27, 28].

The partial branching fractions for $B^\pm \rightarrow K^\pm f_0(980)$ measured in the $K^\pm K^\pm K^\mp$ and $K^\pm \pi^\pm \pi^\mp$ final states are related by the ratio

$$R = \frac{\mathcal{B}(f_0(980) \rightarrow K^+ K^-)}{\mathcal{B}(f_0(980) \rightarrow \pi^+ \pi^-)} = \frac{3}{4} \frac{I_K g_K}{I_\pi g_\pi}, \quad (9)$$

where $3/4$ is an isospin factor, and I_K/I_π is the ratio of the integrals of the square of the $f_0(980)$ amplitude

TABLE I: The magnitudes and phases of the decay coefficients, fit fractions, two-body branching fractions, CP asymmetries, symmetric 90% confidence level CP asymmetry intervals around the nominal value, and the phase differences between the charge-dependent decay coefficients for the individual components of the isobar model fit.

Comp.	ρ	ϕ (rad)	F (%)	$F \times \mathcal{B}(B^\pm \rightarrow K^\pm K^\pm K^\mp)$	A	$(A_{\min}, A_{\max})_{90\%}$	$\delta\phi$ (rad)
$\phi(1020)$	1.66 ± 0.06	$2.99 \pm 0.20 \pm 0.06$	$11.8 \pm 0.9 \pm 0.8$	$(4.14 \pm 0.32 \pm 0.33) \times 10^{-6}$	$0.00 \pm 0.08 \pm 0.02$	$(-0.14, 0.14)$	$-0.67 \pm 0.28 \pm 0.05$
$f_0(980)$	5.2 ± 1.0	$0.48 \pm 0.16 \pm 0.08$	$19 \pm 7 \pm 4$	$(6.5 \pm 2.5 \pm 1.6) \times 10^{-6}$	$-0.31 \pm 0.25 \pm 0.08$	$(-0.72, 0.12)$	$-0.20 \pm 0.16 \pm 0.04$
$X_0(1550)$	8.2 ± 1.1	$1.29 \pm 0.10 \pm 0.04$	$121 \pm 19 \pm 6$	$(4.3 \pm 0.6 \pm 0.3) \times 10^{-5}$	$-0.04 \pm 0.07 \pm 0.02$	$(-0.17, 0.09)$	$0.02 \pm 0.15 \pm 0.05$
$f_0(1710)$	1.22 ± 0.34	$-0.59 \pm 0.25 \pm 0.11$	$4.8 \pm 2.7 \pm 0.8$	$(1.7 \pm 1.0 \pm 0.3) \times 10^{-6}$	$0.0 \pm 0.5 \pm 0.1$	$(-0.66, 0.74)$	$-0.07 \pm 0.38 \pm 0.08$
χ_{c0}^I	0.437 ± 0.039	$-1.02 \pm 0.23 \pm 0.10$	$3.1 \pm 0.6 \pm 0.2$	$(1.10 \pm 0.20 \pm 0.09) \times 10^{-6}$	$0.19 \pm 0.18 \pm 0.05$	$(-0.09, 0.47)$	$0.7 \pm 0.5 \pm 0.2$
χ_{c0}^{II}	0.604 ± 0.034	0.29 ± 0.20	6.0 ± 0.7	$(2.10 \pm 0.24) \times 10^{-6}$	-0.03 ± 0.28	-	-0.4 ± 1.3
NR	13.2 ± 1.4	0	$141 \pm 16 \pm 9$	$(5.0 \pm 0.6 \pm 0.4) \times 10^{-5}$	$0.02 \pm 0.08 \pm 0.04$	$(-0.14, 0.18)$	0

given by Eq. (5) over the $B \rightarrow KKK$ and $B \rightarrow K\pi\pi$ Dalitz plots, and g_K/g_π is the ratio of the $f_0(980)$ coupling constants to $K\bar{K}$ and $\pi\pi$. Using our results and those in Ref. [20], we get $R = 0.69 \pm 0.32$, where we have combined the statistical and systematic errors of the two measurements in quadrature. This is consistent with $R = 0.92 \pm 0.07$, which we get by evaluating the right-hand side of Eq. (9) using the values of the $f_0(980)$ parameters reported by the BES collaboration [23].

V. PARTIAL-WAVE ANALYSES

We further study the nature of the dominant S -wave component by considering the interference between the low-mass and the high-mass scattering amplitudes in the region $m_{23} \in (1.1, 1.8) \text{ GeV}/c^2$, $m_{13} > 2 \text{ GeV}/c^2$. The matrix element is modeled as

$$\mathcal{M} = \frac{\rho_S(s_{23})}{\sqrt{2}} e^{i\phi_S(s_{23})} + \frac{\rho_{\text{NR}}}{\sqrt{2}} e^{-\alpha s_{13}}, \quad (10)$$

where ρ_S and ϕ_S refer to the S -wave and are taken to be constant within each bin of the s_{23} variable and the non-resonant amplitude parameterization is taken from the fit to the high-mass region. The partial-wave expansion truncated at the S -wave describes the data adequately; the magnitude of the S -wave in each bin is readily determined. Because of the mass dependence of the non-resonant component, the phase of the S -wave can also be determined, albeit with a sign ambiguity and rather large errors for bins with a small number of entries or small net variation of the nonresonant component.

The results are shown in Fig. 4, with the S -wave component of the isobar model fit overlaid for comparison. Continuity requirements allow us to identify two possible solutions for the phase; the solution labeled by black squares is consistent with a rapid counterclockwise motion in the Argand plot around $m(K^+K^-) = 1.55 \text{ GeV}/c^2$, which is accommodated in the isobar model as the contribution of the $X_0(1550)$.

Isospin symmetry relates the measurements in $B^\pm \rightarrow K^\pm K^\pm K^\mp$ and $B^0 \rightarrow K^+K^-K_S^0$ [29]. Our results for the K^+K^- S -wave can therefore be used to estimate a potentially significant source of uncertainty in the measurements of $\sin 2\beta$ in $B^0 \rightarrow \phi(1020)K_S^0$ [30, 31] due to the

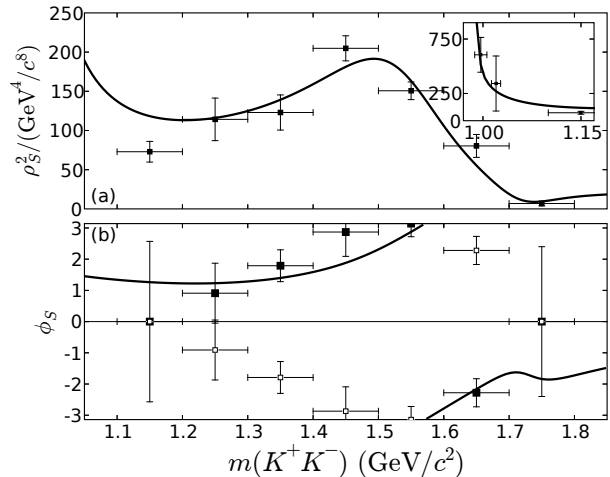


FIG. 4: The results of the partial-wave analysis of the K^+K^- S -wave: (a) magnitude squared, (b) phase. The discrete ambiguities in the determination of the phase give rise to two possible solutions labeled by black and white squares. The curves correspond to the S -wave component from the isobar model fit. The inset shows the evidence of a threshold enhancement from the fits of the S -wave in the vicinity of the K^+K^- threshold and in the region around the $\phi(1020)$ resonance.

contribution of a CP -even S -wave amplitude. We perform a partial-wave analysis in the region $m_{23}(K^+K^-) \in (1.013, 1.027) \text{ GeV}/c^2$, which we assume to be dominated by the low-mass P -wave, due to the contribution of the $\phi(1020)$ resonance, and a low-mass S -wave. The matrix element is modeled as

$$\mathcal{M} = \frac{\rho_S}{\sqrt{2}} + \frac{\rho_P(s_{23})}{\sqrt{2}} e^{i\phi_P(s_{23})} \cos \theta_{13}, \quad (11)$$

where the low-mass S -wave is taken to be constant over the small s_{23} interval considered. The fit results for the P -wave are shown in Fig. 5, with a Breit-Wigner fit of the $\phi(1020)$ resonance overlaid for comparison. For the S -wave we get $\rho_S^2 = (3.4 \pm 2.5) \times 10^2 \text{ GeV}^{-4} c^8$ and compute its fraction in this region using Eq. (7) to be $(9 \pm 6)\%$.

We also consider the region $2m_{K^+} < m(K^+K^-) < 1.006 \text{ GeV}/c^2$, in the immediate vicinity of the K^+K^- threshold. The contribution of the $\phi(1020)$ resonance

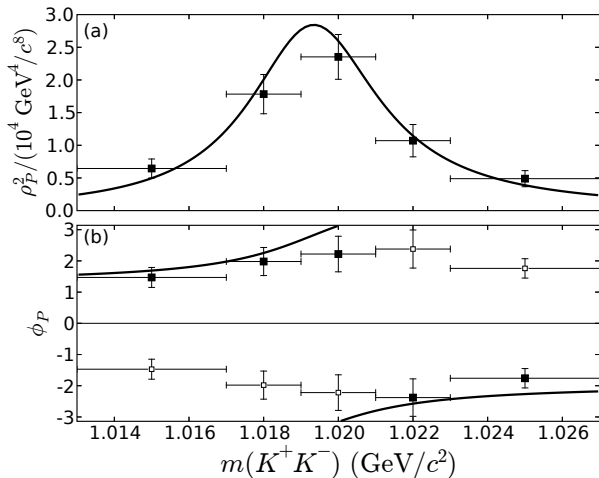


FIG. 5: The results of the partial-wave analysis in the $\phi(1020)$ region for the P -wave: (a) magnitude squared, (b) phase. The discrete ambiguities in the determination of the phase give rise to two possible solutions labeled by black and white squares. The curve corresponds to a Breit-Wigner fit of the $\phi(1020)$ resonance.

tail in this region is suppressed by the centrifugal barrier and is estimated to be smaller than 10%. We fit $\rho_S^2 = (6.1 \pm 1.6) \times 10^2 \text{ GeV}^{-4} c^8$ for the magnitude of the S -wave in this region. The fits in the vicinity of the K^+K^- threshold and in the region around the $\phi(1020)$ resonance indicate a threshold enhancement of the S -wave, which is accommodated in the isobar model by the contribution of the $f_0(980)$ resonance as shown in the inset of Fig. 4.

VI. CONCLUSIONS

In conclusion, we have measured the total branching fraction and the CP asymmetry in $B^\pm \rightarrow K^\pm K^\pm K^\mp$. An

isobar model Dalitz plot fit and a partial-wave analysis of the K^+K^- S -wave show evidence of large contributions from a broad $X_0(1550)$ scalar resonance, a mass-dependent nonresonant component, and an $f_0(980)$ resonance. The ratio of $B^\pm \rightarrow K^\pm f_0(980)$ two-body branching fractions measured by *BABAR* in $B^\pm \rightarrow K^\pm \pi^\pm \pi^\mp$ and $B^\pm \rightarrow K^\pm K^\pm K^\mp$ is consistent with the measurement of g_K/g_π by the BES collaboration, albeit with large errors. Our isobar model fit results are substantially different from those obtained in Ref. [12] due to the larger fitted width of the $X_0(1550)$ and the inclusion of the $f_0(980)$ component in the isobar model. Our results for the $\mathcal{B}(B^\pm \rightarrow K^\pm \phi(1020))$ and $\mathcal{B}(B^\pm \rightarrow K^\pm \chi_{c0})$ branching fractions are in agreement with the previous results from *BABAR* [10, 11], which they supersede, and from other experiments [12, 27, 28]. We have measured the CP asymmetries and the phase differences between the charge-dependent decay coefficients for the individual components of the isobar model and found no evidence of direct CP violation.

We wish to dedicate this paper to Prof. Richard E. (Dick) Dalitz, inventor of the “Phase Space Plot” (as he called it) with which his name is so intimately linked, in tribute as much to his qualities as a gentleman as to his gifts as a physicist.

We are grateful for the excellent luminosity and machine conditions provided by our PEP-II colleagues, and for the substantial dedicated effort from the computing organizations that support *BABAR*. The collaborating institutions wish to thank SLAC for its support and kind hospitality. This work is supported by DOE and NSF (USA), NSERC (Canada), IHEP (China), CEA and CNRS-IN2P3 (France), BMBF and DFG (Germany), INFN (Italy), FOM (The Netherlands), NFR (Norway), MIST (Russia), and PPARC (United Kingdom). Individuals have received support from CONACyT (Mexico), Marie Curie EIF (European Union), the A. P. Sloan Foundation, the Research Corporation, and the Alexander von Humboldt Foundation.

-
- [1] D. Du, H. Gong, J. Sun, D. Yang, and G. Zhu, *Phys. Rev.* **D65**, 094025 (2002).
 - [2] M. Beneke and M. Neubert, *Nucl. Phys.* **B675**, 333 (2003).
 - [3] C. Chen, Y. Keum, and H. Li, *Phys. Rev.* **D64**, 112002 (2001).
 - [4] P. Colangelo, F. de Fazio, and T. Pham, *Phys. Lett.* **B542**, 71 (2002).
 - [5] D. Du, J. Sun, D. Yang, and G. Zhu, *Phys. Rev.* **D67**, 014023 (2003).
 - [6] N. de Groot, W. Cottingham, and I. Wittingham, *Phys. Rev.* **D68**, 113005 (2003).
 - [7] B. Aubert et al. (*BABAR* Collaboration), *Nucl. Instrum. Meth.* **A479**, 1 (2002).
 - [8] PEP-II: An Asymmetric B Factory. Conceptual Design Report. SLAC-418, 1993.
 - [9] B. Aubert et al. (*BABAR* Collaboration), *Phys. Rev. Lett.* **91**, 051801 (2003).
 - [10] B. Aubert et al. (*BABAR* Collaboration), *Phys. Rev.* **D69**, 011102 (2004).
 - [11] B. Aubert et al. (*BABAR* Collaboration), *Phys. Rev.* **D69**, 071103 (2004).
 - [12] A. Garmash et al. (Belle Collaboration), *Phys. Rev.* **D71**, 092003 (2005).
 - [13] H. Albrecht et al. (ARGUS Collaboration), *Z. Phys.* **C48**, 543 (1990).
 - [14] G. Fleming, *Phys. Rev.* **135**, B551 (1964).
 - [15] D. Morgan, *Phys. Rev.* **166**, 1731 (1968).
 - [16] M. Baubillier et al., *Z. Phys.* **C17**, 309 (1983).
 - [17] D. Aston et al., *Nucl. Phys.* **B301**, 525 (1988).
 - [18] S. Eidelman et al. (Particle Data Group), *Phys. Lett.* **B592** (2004).

- [19] P. Minkowski and W. Ochs, Eur. Phys. Jour. **C39**, 71 (2005).
- [20] B. Aubert et al. (*BABAR* Collaboration), Phys. Rev. **D72**, 072003 (2005).
- [21] J. Blatt and V. Weisskopf, *Theoretical Nuclear Physics* (J. Wiley, New York, 1952).
- [22] J. Link et al. (FOCUS Collaboration), Phys. Lett. **B621**, 72 (2005).
- [23] M. Ablikim et al. (BES Collaboration), Phys. Lett. **B607**, 243 (2005).
- [24] K. Y. H. Cheng, Phys. Rev. **D66**, 054015 (2002).
- [25] S. Fajfer, T. Pham, and A. Protopotnik, Phys. Rev. **D70**, 034033 (2004).
- [26] See EPAPS Document No. [to be assigned] for the fit fractions of the interference terms and the fit parameters correlation matrix. For more information on EPAPS, see <http://www.aip.org/pubservs/epaps.html>.
- [27] R. Briere et al. (CLEO Collaboration), Phys. Rev. Lett. **86**, 3718 (2001).
- [28] D. Acosta et al. (CDF Collaboration), Phys. Rev. Lett. **95**, 031801 (2005).
- [29] M. Gronau and J. Rosner, Phys. Rev. **D72**, 094031 (2005).
- [30] B. Aubert et al. (*BABAR* Collaboration), Phys. Rev. **D71**, 091102 (2005).
- [31] K. Abe et al. (Belle Collaboration), Phys. Rev. Lett. **91**, 261602 (2003).

TABLE I: Fit fractions matrix of the best fit. The diagonal elements F_{kk} correspond to component fit fractions shown in the paper in Table I. The off-diagonal elements give the fit fractions of the interference terms defined as $F_{kl} = 2\Re \int \mathcal{M}_k \mathcal{M}_l^* ds_{23} ds_{13} / \int |\mathcal{M}|^2 ds_{23} ds_{13}$.

$F_{kl} \times 100\%$	ϕ	$f_0(980)$	$X_0(1550)$	$f_0(1710)$	χ_{c0}	NR
ϕ	11.8 ± 0.9 ± 0.8	-0.94 ± 0.18 ± 0.11	-1.71 ± 0.36 ± 0.24	0.01 ± 0.10 ± 0.03	0.11 ± 0.02 ± 0.05	3.54 ± 0.38 ± 0.40
$f_0(980)$		19 ± 7 ± 4	53 ± 12 ± 7	-4.5 ± 2.9 ± 1.2	-0.9 ± 0.2 ± 0.5	-85 ± 21 ± 14
$X_0(1550)$			121 ± 19 ± 6	-30 ± 11 ± 4	-1.1 ± 0.3 ± 0.5	-140 ± 26 ± 7
$f_0(1710)$				4.8 ± 2.7 ± 0.8	-0.10 ± 0.07 ± 0.07	4 ± 6 ± 3
χ_{c0}					3.1 ± 0.6 ± 0.2	3.9 ± 0.4 ± 1.9
NR						141 ± 16 ± 9

TABLE II: Fit parameters correlation matrix of the best fit.

	ϕ		$f_0(980)$		$X_0(1550)$				$f_0(1710)$		χ_{c0}		NR	
	ρ	ϕ	ρ	ϕ	ρ	ϕ	m_0	Γ_0	ρ	ϕ	ρ	ϕ	ρ	α
	1	2	3	4	5	6	7	8	9	10	11	12	13	14
1	1.00	-0.10	-0.14	0.01	0.00	-0.00	0.02	-0.00	-0.00	0.01	-0.01	0.01	-0.09	-0.07
2	-0.10	1.00	0.69	0.61	0.38	-0.42	-0.64	0.46	0.03	-0.20	0.02	-0.29	0.34	0.21
3	-0.14	0.69	1.00	0.72	0.33	-0.63	-0.44	0.37	0.05	-0.37	0.05	-0.30	0.73	0.49
4	0.01	0.61	0.72	1.00	0.68	-0.80	-0.50	0.67	0.19	-0.51	0.07	-0.41	0.70	0.56
5	0.00	0.38	0.33	0.68	1.00	-0.52	-0.14	0.94	0.45	-0.59	0.05	-0.42	0.46	0.41
6	-0.00	-0.42	-0.63	-0.80	-0.52	1.00	0.39	-0.63	0.28	0.75	-0.02	0.30	-0.52	-0.29
7	0.02	-0.64	-0.44	-0.50	-0.14	0.39	1.00	-0.30	0.25	0.05	-0.01	0.14	-0.07	0.00
8	-0.00	0.46	0.37	0.67	0.94	-0.63	-0.30	1.00	0.17	-0.63	0.04	-0.39	0.34	0.26
9	-0.00	0.03	0.05	0.19	0.45	0.28	0.25	0.17	1.00	0.04	0.05	-0.19	0.36	0.42
10	0.01	-0.20	-0.37	-0.51	-0.59	0.75	0.05	-0.63	0.04	1.00	0.00	0.22	-0.39	-0.20
11	-0.01	0.02	0.05	0.07	0.05	-0.02	-0.01	0.04	0.05	0.00	1.00	0.40	0.10	0.17
12	0.01	-0.29	-0.30	-0.41	-0.42	0.30	0.14	-0.39	-0.19	0.22	0.40	1.00	-0.35	-0.30
13	-0.09	0.34	0.73	0.70	0.46	-0.52	-0.07	0.34	0.36	-0.39	0.10	-0.35	1.00	0.92
14	-0.07	0.21	0.49	0.56	0.41	-0.29	0.00	0.26	0.42	-0.20	0.17	-0.30	0.92	1.00

TABLE III: Phase differences matrix of the best fit. The matrix elements are defined as $\phi_{kl} = \phi_l - \phi_k$. The last row corresponds to the results of the best fit shown in the paper in Table I. The other phase differences are derived from the fit results.

ϕ_{kl}	ϕ	$f_0(980)$	$X_0(1550)$	$f_0(1710)$	χ_{c0}	NR
ϕ	0	-2.51 ± 0.17 ± 0.11	-1.70 ± 0.27 ± 0.07	2.71 ± 0.35 ± 0.13	2.27 ± 0.35 ± 0.12	-2.99 ± 0.20 ± 0.06
$f_0(980)$	2.51 ± 0.17 ± 0.11	0	0.81 ± 0.25 ± 0.12	-1.07 ± 0.36 ± 0.17	-1.50 ± 0.33 ± 0.17	-0.48 ± 0.16 ± 0.08
$X_0(1550)$	1.70 ± 0.27 ± 0.07	-0.81 ± 0.25 ± 0.12	0	-1.88 ± 0.19 ± 0.09	-2.32 ± 0.22 ± 0.09	-1.29 ± 0.10 ± 0.04
$f_0(1710)$	-2.71 ± 0.35 ± 0.13	1.07 ± 0.36 ± 0.17	1.88 ± 0.19 ± 0.09	0	-0.44 ± 0.30 ± 0.13	0.59 ± 0.25 ± 0.11
χ_{c0}	-2.27 ± 0.35 ± 0.12	1.50 ± 0.33 ± 0.17	2.32 ± 0.22 ± 0.09	0.44 ± 0.30 ± 0.13	0	1.02 ± 0.23 ± 0.10
NR	2.99 ± 0.20 ± 0.06	0.48 ± 0.16 ± 0.08	1.29 ± 0.10 ± 0.04	-0.59 ± 0.25 ± 0.11	-1.02 ± 0.23 ± 0.10	0